Mesoporous biohybrid epichlorohydrin crosslinked chitosan/carbon–clay adsorbent for effective cationic and anionic dyes adsorption

F. Marrakchi [a], B.H. Hameed [b,*], E.H. Hummadi [c]

[a] School of Energy and Power Engineering, Jiangsu University, Jiangsu 212013, China
[b] Department of Chemical Engineering, College of Engineering, Qatar University, P.O. Box 2713, Doha, Qatar
[c] Department of Biotechnology, College of Science, University of Diyala, Baqubah, Iraq

ARTICLE INFO

ABSTRACT

Epichlorohydrin crosslinked chitosan/carbon–clay (CSCC) biohybrid adsorbent was prepared for the adsorption of cationic methylene blue (MB) and anionic azo acid blue 29 (AB 29). The 40:60 wt% of chitosan (CS) and carbon–clay (CC) was selected as the best biohybrid adsorbent (CS40CC60) for the adsorption of both dyes. The adsorption of MB and AB 29 on CS40CC60 was carried out in a batch process to investigate the effects of initial dye concentration (25–400 mg/L), initial pH (3−11), contact time and adsorption temperature (30, 40 and 50 °C). The kinetics results of dyes adsorption onto CS40CC60 fit well to the pseudo-second-order model. The iso-therms analysis demonstrated that the Freundlich isotherm described the adsorption data, and the q_{max} (mg/g) were 95.31 for MB and 167.35 for AB29 at 50 °C. These findings reveal the potential and effectiveness of the newly prepared biohybrid adsorbent for the adsorption of both dyes.

1. Introduction

Pollution is an enormous challenge faced by societies today. The rapid increase of industrialization, modernization, and the human population have caused large-scale pollution and severe global issues with considerable impact on countries, economies, and the overall environment. Water pollution represent a biggest threat of life on the planet and poses the next largest risk after air pollution [1]. It not only poses risks to 2.1 million lives per year because of water-related illness and mortality but also threatens the life of numerous flora and fauna species, thereby causing the loss of biodiversity [2]. The influx of significant quantities of industrial wastewater into freshwater without proper treatment causes clean water contamination. Synthetic colored substances is the first dangerous well-known water pollutant that causes major calamity and is a threat to water-dependent bodies [3].

Given the importance of color stuff removal from wastewater, treatment before the eventual release of colored effluents from dye-utilizing industries into the environment is a key task. Thus, effective methods to control and manage dye-containing wastewater are prioritized. Biological treatment, coagulation/flocculation, filtration, and photocatalytic degradation are feasible dye removal methods [4]. However, these remediation technologies are difficult to implement, ineffective at high concentrations, and costly at US$10–450 per m³ of treated water [5]. Adsorption is an effective, successful, and economical technique used to clean up contaminated water. Commercial activated carbons (CACs) are versatile and unique adsorbents for colored wastewater purification due to its excellent surface reactivity, high surface area, superior adsorption capacity and physicochemical stability [6]. CACs world demand is increasing and expected to exceed more than US$ 10.50 billion by 2024 [7]. CACs are traditionally produced from coal as a non-renewable carbon source. Besides, elevated energy is consumed for CACs production, restricted its intensive use. Thus, there is a growing focus on finding low-cost carbon from biomaterials to serve as an alternative source to CACs.

Chitosan is a polymer containing hydroxyl (–OH) and amino (−NH₂) functional groups [8,9]. The utilization of chitosan as a bio-based adsorbent to remove artificial colors is limited by the formation of colloid in water, solubility in acid, degradation by chemical actions and low surface area [10]. Cross-linking technique can improve chitosan stability in acidic environment and strengthens its mechanical properties for uptake [11–13].

Tons of spent bleaching sorbent generated per year in olive and vegetable oil refineries have been disposed into the surrounding territorials. Spent bleaching sorbent contains approximately 37.45% SiO₂ and 8.01% Al₂O₃, which represent an essential constituent of clay, as well as 26.99% retained oil which can be carbonized into valuable commodity carbon [14]. Thus, spent bleaching sorbent is a good precursor for carbon–clay (CC) adsorbent [15].

Considering the low adsorption capacity of chitosan to basic dyes [11] and spent bleaching sorbent to anionic dyes [15], this work aims to synthesize epichlorohydrin crosslinked chitosan/carbon–clay

* Corresponding author.
  E-mail address: b.hammadi@qu.edu.qa (B.H. Hameed).

(CSCC) biohybrid adsorbent for the adsorption of cationic and acid azo dyes. The basic methylene blue (MB) and the anionic azo acid blue 29 (AB29) were used as model adsorbates to evaluate the adsorption effectiveness of the CSCC.

2. Materials and methods

2.1. Materials

Spent bleaching sorbent (SBS) was obtained from a local refinery of olive oil in Sfax, Tunisia. Chitosan (CS) was provided by a pharmaceutical company, Malaysia. Acetic acid ($C_2H_4O_2$, >99% purity), hydrochloric acid (HCl, 37% purity), epichlorohydrin (C_3H_5ClO, >99% purity), and sodium hydroxide (NaOH, >99% purity) were supplied by R&M Chemicals, Malaysia and used as received. Anionic azo acid blue 29 ($C_{22}H_{14}N_6Na_2O_9S_2$, AB 29) and cationic methylene blue ($C_{16}H_{18}ClN_3S^*x$ H_2O (x = 2–3), MB) were purchased from Sigma–Aldrich and Merck, respectively.

2.2. Preparation of carbon-clay: carbonization of spent bleaching sorbent

Carbonization of spent bleaching sorbent (SBS) to prepare a carbon–clay (CC) material was described previously in detail [15]. An amount of 100 g of SBS was carbonized under a flow of 100 mL/min N_2 gas (99%) at 500 °C for 1 h. The resulting CC was washed with 0.10 mol/L HCl solution and then with distilled water until the elution solution pH reaches 7.

2.3. Preparation of crosslinked chitosan/carbon-clay biohybrid adsorbent

The dissolution of 2 g of powdered chitosan (CS) in acetic acid aqueous solution (5% v/v, 150 mL) was carried out at ambient conditions and the mixture was gently stirred till homogeneity. The prepared carbon–clay material (CC) was added, and the mixture was stirred, beaded through a syringe into 1 M NaOH aqueous solution under stirring, and left overnight under continuous stirring. The produced wet CSCC biohybrid beads were washed several times with distilled water to eliminate any remaining NaOH till the elution solution reaches a pH ≈ 7. The produced CSCC beads were added to 100 mL of 1% epichlorohydrin solution and stirred for 6 h at 50 °C. Thereafter, the produced CSCC were rinsed again and subsequently freeze-dried for 48 h. For comparison purpose, freeze-dried CSCC samples were prepared with various wt%, viz., 0:100 wt% (CS0CC100), 20:80 wt% (CS20CC80), 40:60 wt% (CS40CC60), 50:50 wt% (CS50CC50), 60:40 wt% (CS60CC40), 80:20 wt% (CS80CC20), 100:0 wt% (CS100CC0).

2.4. Characterization of adsorbents

Morphological and elemental analysis of the best-selected CSCC hybrid adsorbent was carried out by FE–SEM LEO SUPRA 35VP coupled with EDX spectrometer.

The Brunauer–Emmett–Teller model surface area (S_{BET}) was measured using N_2 adsorption/desorption isotherm measured at −196 °C using Micromeritics ASAP 2020 instrument. The external surface area (S_{ext}) surface area of micropore (S_{micro}) and the volume of micropore (V_{micro}) were calculated via the t-plot technique. The surface area of mesopore (S_{meso}), and the volume of mesopore (V_{meso}) were determined by the method of Barrett-Joyner-Halenda (BJH). The V_T (volume of total pore) was estimated to be the liquid volume of N_2 at high relative pressure (P/P_0 ~ 0.99). The distribution of pore size was measured by the BJH model, and the D_P (mean pore diameter) was calculated from $D_P = 4V_T/S_{BET}$. FTIR spectra of best CSCC before and after dyes adsorption were obtained by a Perkin Elmer Spectrum GX Infrared Spectrometer from 4000 to 400 cm^{-1} using the KBr disk method at ambient temperature. The point of zero charges (pH_{pzc}) for the best CSCC adsorbent was determined following the method described by Benhouria et al. [16].

2.5. Batch adsorption experiments

All the adsorption runs were done in a batch process using a thermostated shaker (Model Protech, Malaysia) at 150 rpm. Firstly, to determine the best biohybrid adsorbent, 0.10 g of each sample (CS100CC0, CS80CC20, CS60CC40, CS50CC50, CS40CC60, CS20CC80, and CS0CC100) was added to 100 mL of 100 mg/L MB and AB29 and were stirred at 30 °C. Secondly, the effect of best hybrid dosage (W) was evaluated between 0.10 and 0.30 g. Moreover, initial pH effect (3.0 to 11.0), adjusted with 0.10 mol/L of HCl or NaOH, was performed using initial dye concention (C_0) of 100 mg/L at 30 °C. Kinetic studies were conducted at different contact times (0 to 26 h) using 200 mL dye solution volume (V) and C_0 of 25, 50, 100, 200, 300, and 400 mg/L at 30 °C. Finally, equilibrium studies were similar to the kinetics procedure except that the samples were taken at equilibrium at different temperatures of 30, 40 and 50 °C. After each experiment, the remaining concentration was spectrophotometrically determined at 602 nm for AB 29 and 665 nm for MB (Shimadzu UV–1601). The adsorbed amount of dyes q_t (mg/g) at time t (min), and equilibrium, q_e (mg/g), are expressed, respectively, by Eqs. (1) and (2).

$$q_t = \frac{V}{W} (C_0 - C_t) \tag{1}$$

$$q_e = \frac{V}{W} (C_0 - C_e) \tag{2}$$

3. Results and discussion

3.1. Optimization of CSCC biohybrid adsorbent

The MB and AB 29 removal (%) were calculated using different prepared adsorbents (CS100CC0, CS80CC20, CS60CC40, CS50CC50, CS40CC60, CS20CC80 and CS0CC100) in order to find the best adsorbent (Fig. 1). It was noticed when the wt% CC increase, the % removal of AB 29 decrease while that of MB increase. The biohybrid adsorbent with 40:60 wt% of CS and CC (CS40CC60) showed high dyes removal and therefore was chosen as the best biohybrid adsorbent.

3.2. Characterization of CS, CC, and CSCC

Magnified micrographs at 3000× of CS, CC, and CS40CC60 are shown in Fig. 2. Chitosan (CS) shows a stacked microsheet like a rough non–porous rock structure (Fig. 2a). From Fig. 2b, it is shown that the carbon–clay (CC) surface displays porous texture due to the
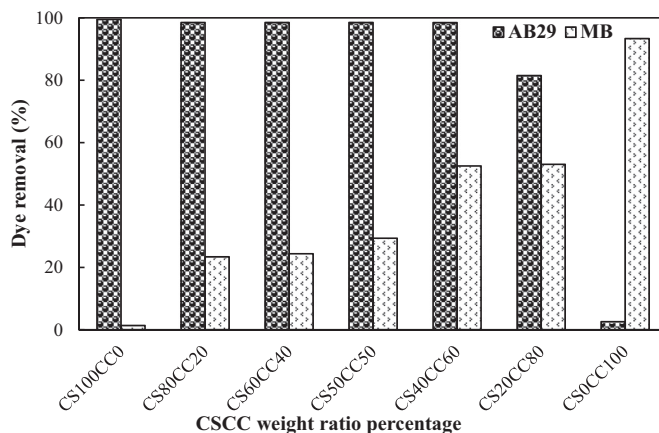

Fig. 1. AB 29 and MB removal % by CSCC biohybrids with different wt% at C_0 = 0.10 g/L, m/V = 1 g/L, and t = 26 h.
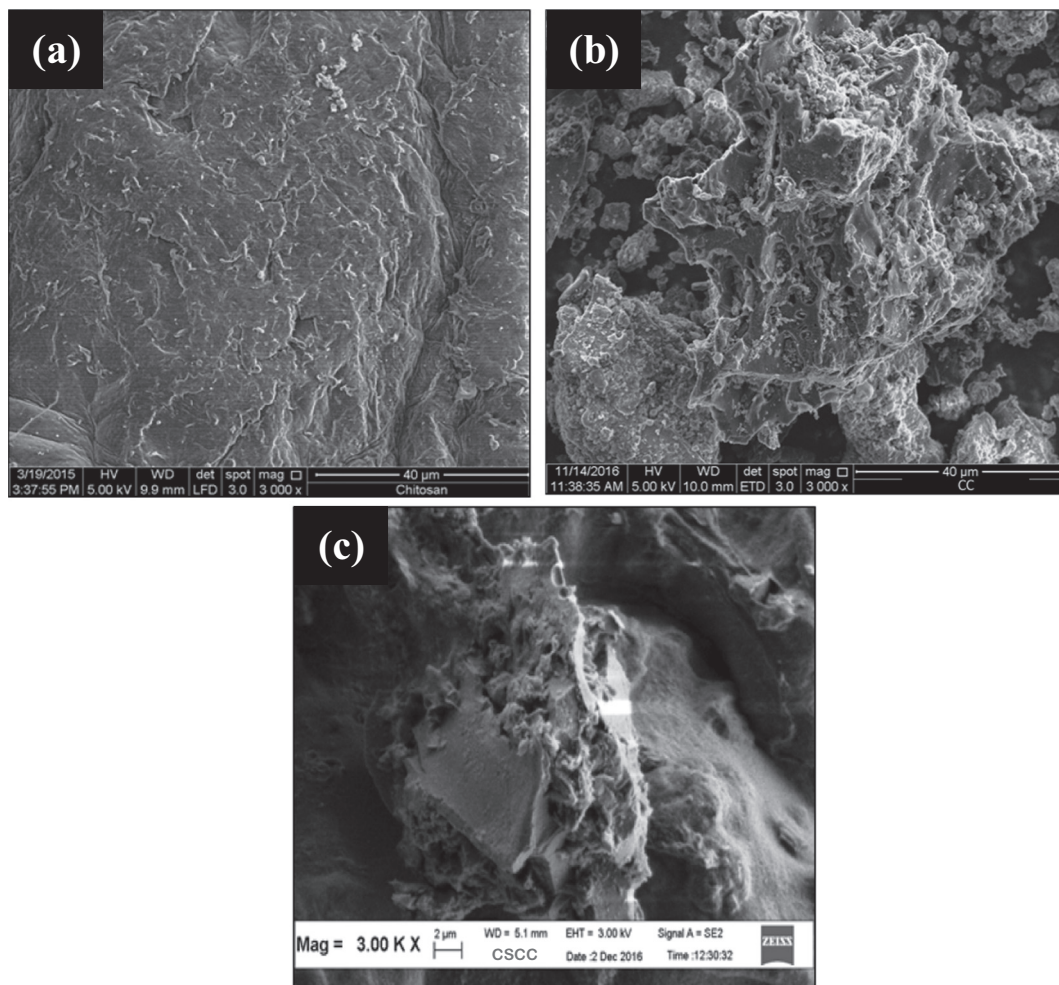
Fig. 2. Images of SEM at 3000× magnification of (a) CS, (b) CC, and (c) CS40CC60.

carbonization of SBS and the brunt of retained oil, resulting in the loss of volatile compounds and the release of CO and CO_2 [15]. After crosslinking, it is seen that the CC interlayer spaces (Fig. 2b) are reduced compared to CS40CC60 (Fig. 2c). The same aspect was noticed by comparing the textural parameters of CC and CS40CC60 (Table 1) where S_{BET}, V_T, and D_p of CC decreased after crosslinking, respectively, from 168.45 to 18.41 m^2/g, 0.2875 to 0.0238 cm^3/g, and 6.02 to 4.41 nm. This could be ascribed to the fact that chitosan was partially and/or fully blocked the carbon-clay pores through the interaction of -NH_2 groups in CS and CC layers particles. The result was similar to the reported in the literature where the surface porosity decreases when chitosan assembled on AuNPs/Clay and AgNPs/Clay [17] and chitosan coating on calcium alginate [18] and zeolite [19], and chitosan grafting to palygorskite [20].

EDX analysis results of CS, CC and CS40CC60 are listed in Table 2. The major elements in carbon-clay (CC) were C, O, Mg, Al, Si, K, Ca, and Fe and originating from its virgin composition of bleaching earth and activated carbon used as adsorbents in the olive oil refining process. EDX spectra of the CS40CCC60 in Table 2 confirms that the CC and CS are fully integrated.

FTIR spectra obtained for CS40CC60 adsorbent before and after dyes adsorption is given in Fig. 3. In the spectra of all three samples, bands around 3294.24–3288.43 cm^{-1}, 2874.03–2873.05 cm^{-1}, 1593.61–1592.63 cm^{-1}, 1378.22–1374.33 cm^{-1}, 1016.03–1015.58 cm^{-1} are identical to the functional groups of CS [10,11] and CC [15].These bands are assigned, respectively, to vibrations of OH and NH stretching, C=H stretching, aromatic C—H stretching, conjugated C=C stretching or N—H deformation, C—O or Si—O stretching. FTIR spectra comparison of AB 29 and MB dye adsorbed CS40CC60 to the fresh CS40CC60 revealed the slightly decrease in peaks intensity and absorbance and shift of some others, confirming the possible involvement of such functional groups on the surface of the CS40CC60 during the adsorption process.

3.3. Effect of CS60CC40 dosage

The effect of CS60CC40 adsorbent dosage on dyes removal was studied (figure not shown), and the % removal of MB and AB29 at 0.10, 0.20 and 0.30 g were 52.52% and 98.48%, 76.78% and 99.10%, and 77.24% and 99.50%, respectively. When the dose increased from 1 g/L to 2 g/L, a rapidly increase in both dyes' removal percentage was noticed. This may be due to the larger surface area, and the availability of more active binding sites for adsorbent [21]. However, a further increase in the CS60CC40 dosage >2 g/L did not change the dye removal %. This may be because of surface saturation leading to the unavailability of sites. Thus, 2 g/L of CS60CC40 was considered as the optimum dosage.

3.4. Effect of initial concentration and pH of dye solution

The dyes concentration change (C_t) at various initial dyes concentrations (25–400 mg/L) at 30 °C are shown in Fig. 4a and b. The results indicate that the contact time of uptakes of AB 29 and MB were 30 and

Table 1
Surface area and pore characteristics of CS40CC60.

Adsorbents	BET surface area S_{BET} (m^2/g)	Micropore surface area S_{micro} (m^2/g)	External surface area S_{ext} (m^2/g)	Micropore volume V_{micro} (cm^3/g)	Mesopore volume V_{meso} (cm^3/g)	Total pore volume V_T (cm^3/g)	Average pore width D_P (nm)
CC [15]	168.45	1.73	166.76	0.0006	0.2869	0.2875	6.02
CS40CC60	18.41	0.078	18.33	0.0002	0.0236	0.0238	4.41

Table 2
EDX of (a) CS, (b) CC, and (c) CS40CC60.

Element weight (%)	C	O	N	Al	Si	Mg	K	Ca	Fe
CS	46.93	47.01	6.07	–	–	–	–	–	–
CC	81.33	14.08	–	0.87	2.91	0.18	0.10	0.05	0.48
CS40CC60	55.72	28.20	4.96	2.54	8.57	–	–	–	–

–: not detected.

60 min for the low concentrations and of 630 and 120 min for the high concentrations, respectively. The adsorption removal of AB 29 is greater than MB, and this is due to the electrostatic affinity between the CS40CC60 surfaces and the negatively charged AB 29 dye; the presence of amino-functional groups (–NH$_2$) could dissociate and become positively charged sites.

The increase of MB and AB 29 residual concentration with the increase of C_0 indicates the high dependence of dye uptake on the initial adsorbate concentration. An increase in residual dye concentration

was closely correlated with the mass driving force effect which permit the movement of dyes from the liquid-phase boundary to the adsorbent interface. Thus, this effect can be explained by the intraparticle diffusion mechanism after the saturation of the surface [22,23].

The initial solution pH effect on the adsorption of MB and AB 29 onto CS40CC60 at 30 °C is shown in Fig. 4c. It was seen that the AB 29 adsorption was low at > pH 8 but high at pH 3–8. However, different behavior was noticed for MB. Dye adsorption influenced by pH solution could be explained by zero-point charge (pH$_{pzc}$). The pH$_{pzc}$ of CS40CC60' was 5.61. CS pH$_{pzc}$ exhibits a basic behavior ~9.0 according to the literature [24]. A possible explanation for the decrease of pH$_{pzc}$ could be attributed to the acidic nature of carbon-clay (CC) due to its high affinity to MB (93.36%) compared to the AB29 (2.58%) as shown in Fig. 1, and this acidic behavior tends to decrease through chitosan blending. These findings agree with the pH$_{pzc}$ measured by Gecol et al. [25] (increase in the pHpzc from 2.8 to 5.8 of a kaolinite clay coated with chitosan) and Unuabonah et al. [26] (increase from 5.81 to 7.44 of a zinc-hybrid clay modified with chitosan). This shows that the integrating of the CC
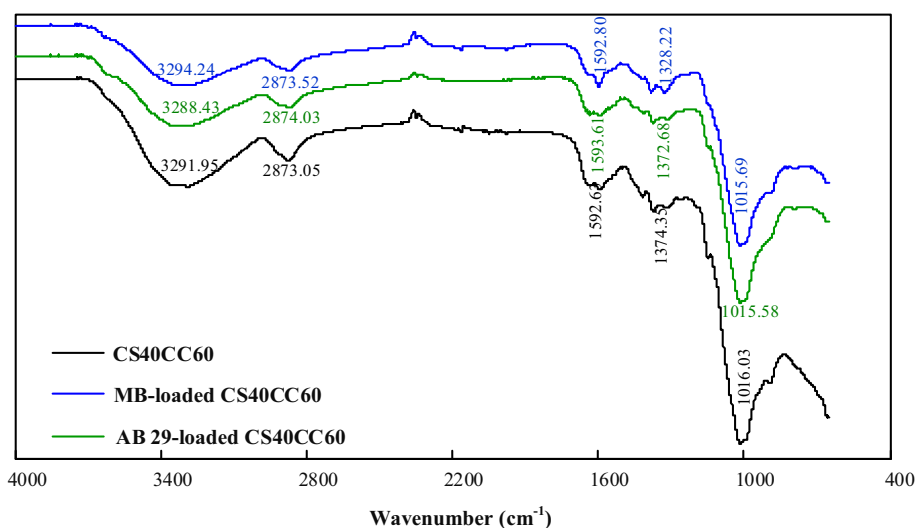

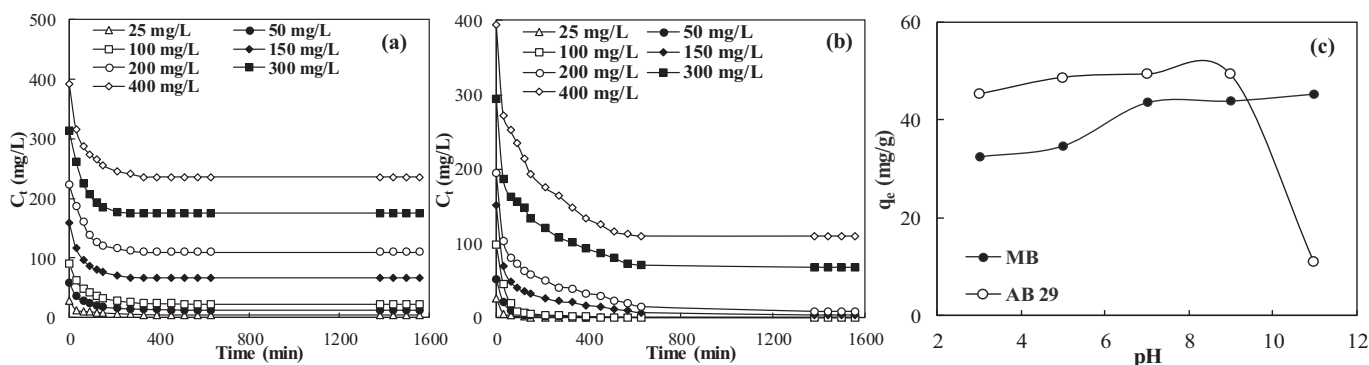**Fig. 3.** FTIR spectra of CS40CC60 before and after dye molecules adsorption.

Fig. 4. (a) MB and (b) AB 29 residual concentration versus time at 30 °C. (c) Effect of initial pH on dyes adsorption onto CS40CC60.

with CS affects the pH_{pzc} of the CS40CC60. At pH < 5.61, protonation of amine (–NH$_2$) groups into ammonium (–NH$_3^+$) groups is undertaken on the surface of CS40CC60 resulting in high anionic dyes adsorption due to the coulomb force attraction between NH$_3^+$ groups of CS and negatively charged AB 29 molecules. However, when the solution pH increase >5.61, deprotonation occurs of NH$_3^+$ groups and back into NH$_2$ groups and therefore lesser adsorption of AB 29 resulting in the repulsion between anionic AB 29 and the surface of CS40CC60 [10,27]. In the case of MB at lower pH, less adsorption uptake is obtained as a result of the competition of MB molecules with protons to bind to OH$^-$ and NH$_2$ groups on the CS40CC60 surface. Nevertheless, in basic medium, a rapid interaction of MB to negative CS40CC60 surface results in high adsorption [11,28].

3.5. Kinetic and isotherm modeling

Kinetics and equilibrium adsorption results for both dyes are presented in Fig. 5(a–b) and (c–d), respectively, and analyzed using the nonlinear model forms of Lagergren's pseudo-first-order [29] (Eq. (3)), pseudo-second-order [30] (Eq. (4)), Langmuir isotherm [31] (Eq. (5)) and Freundlich isotherm [32] (Eq. (6)).

$$q_t = q_e \left(1 - e^{-k_f t}\right) \tag{3}$$

$$q_t = \frac{q_e^2 k_s t}{1 + q_e k_s t} \tag{4}$$

$$q_e = \frac{q_{max} K_L C_e}{1 + K_L C_e} \tag{5}$$

$$q_e = K_F C_e^{1/n} \tag{6}$$

Accuracy of the modeled regression ($q_{e,cal}$) compared to the experimental ($q_{e,exp}$) kinetic and equilibrium data were considered with respect to the R^2 (Eq. (7)), and *RMSE*; root-mean-square error (Eq. (8)).

$$R^2 = 1 - \frac{\sum_{n=1}^n \left(q_{e.\,exp.n} - q_{e.cal.n}\right)^2}{\sum_{n=1}^n \left(q_{e.\,exp.n} - \overline{q_{e.\,exp.n}}\right)^2} \tag{7}$$

$$RMSE = \sqrt{\frac{1}{n-1} \sum_{n=1}^n \left(q_{e.\,exp.n} - q_{e.cal.n}\right)^2} \tag{8}$$

The calculated values of k_f (1/min), k_s (g/(mg.min)), K_L (L/mg), and K_F ((mg/g) (L/mg)$^{1/n}$), q_{max} (mg/g), n, together with R^2 and *RMSE* are listed in Tables 3 and 4.

From Table 3, comparing the experimental values of $q_{e,exp}$ to the $q_{e,cal}$ calculated from Eq. (4) resulted in relatively low *RMSE* (0.17 to 5.68) and high $R^2 \simeq 1$ compared to the Lagergren's model. The obtained rate constants k_f and k_s decreased with increasing C_0. This showed that the adsorption system was concentration-dependent and supported the earlier finding (Section 3.4) that dyes with lower C_0 attained equilibrium faster. The k_f and k_s of AB 29 > MB indicating that the CS40CC60 surface has a greater affinity for AB 29. These obtained results agreed with the previous works conducted on adsorption of AB 29 and MB where the pseudo-second-order model described well the kinetics data [10,15,33–35].
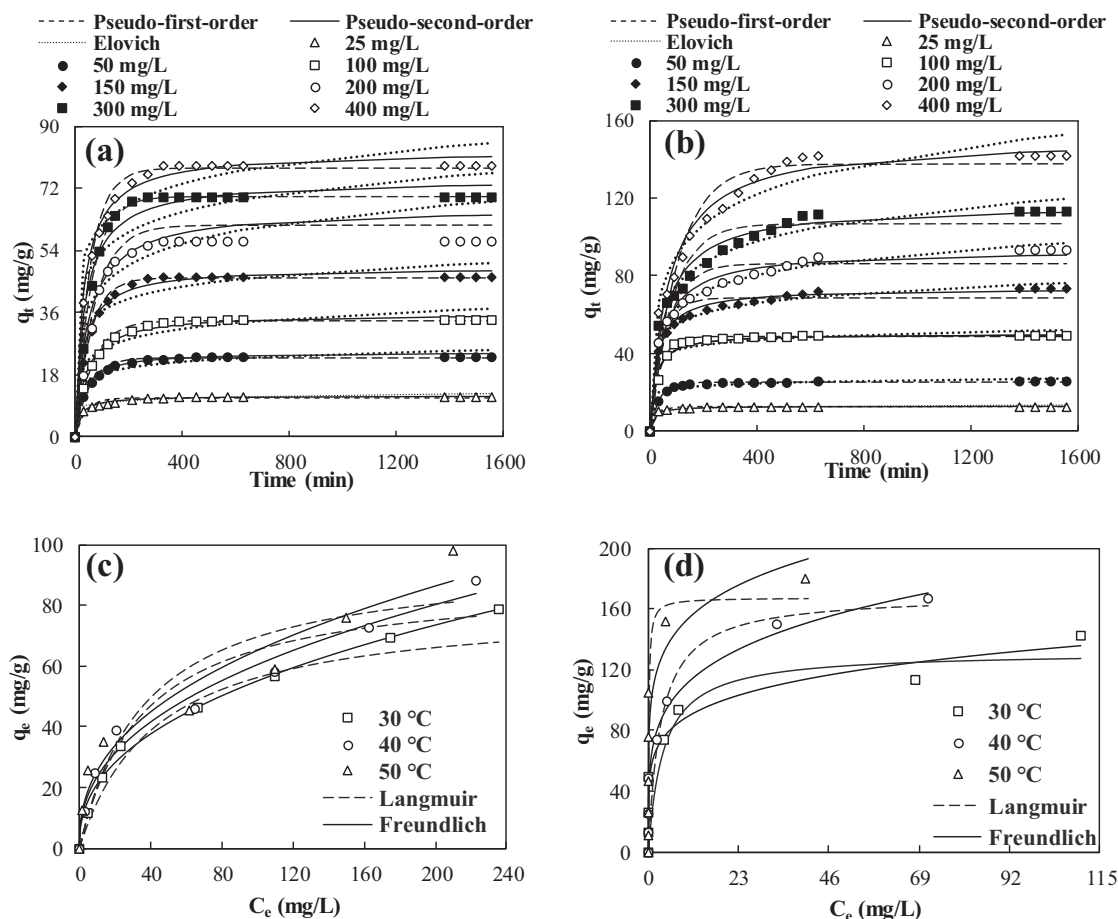

Fig. 5. (a) MB and (b) AB 29 adsorption kinetics at 30 °C. (c) MB and (d) AB 29 adsorption isotherms at 30, 40, and 50 °C.

Table 3
Pseudo-first- and second-order kinetic parameters for methylene blue and acid blue 29 adsorption onto CS40CC60 at 30 °C.

Pseudo-first-order

C_0 AB 29 (mg/L)	$q_{e,exp}$ (mg/g)	$q_{e,cal}$ (mg/g)	k_f (1/min)	R^2	RMSE	C_0 MB (mg/L)	$q_{e,exp}$ (mg/g)	$q_{e,cal}$ (mg/g)	k_s (1/min)	R^2	RMSE
25	12.63	12.35	0.037	0.95	1.88	25	11.73	11.35	0.025	0.94	0.72
50	25.59	25.15	0.029	0.99	0.46	50	23.30	22.91	0.019	0.90	0.66
100	49.21	48.63	0.027	0.99	0.65	100	33.83	33.47	0.015	0.99	0.76
150	73.60	68.81	0.022	0.93	4.52	150	46.29	46.06	0.018	0.99	0.82
200	93.55	85.89	0.015	0.90	7.31	200	56.75	61.22	0.013	0.97	1.21
300	113.57	107.15	0.012	0.91	8.98	300	69.58	69.80	0.016	0.99	0.51
400	142.20	137.88	0.010	0.94	9.14	400	78.75	77.98	0.018	0.99	2.47

Pseudo-second-order

C_0 AB 29 (mg/L)	$q_{e,exp}$ (mg/g)	$q_{e,cal}$ (mg/g)	k_f $\left(\frac{g}{mg.\,,min.}\right)$	R^2	RMSE	C_0 MB (mg/L)	$q_{e,exp}$ (mg/g)	$q_{e,cal}$ (mg/g)	k_s $\left(\frac{g}{mg.\,,min.}\right)$	R^2	RMSE
25	12.63	12.62	0.0056	0.99	0.17	25	11.73	11.96	0.0039	0.99	0.33
50	25.59	26.29	0.0026	0.99	0.54	50	23.30	24.33	0.0013	0.99	0.41
100	49.21	50.09	0.0010	0.98	1.56	100	33.83	35.89	0.0007	0.99	0.88
150	73.60	73.36	0.0005	0.99	1.77	150	46.29	48.91	0.0006	0.99	1.38
200	93.55	93.19	0.0002	0.98	3.60	200	56.75	66.40	0.0003	0.97	3.06
300	113.57	116.49	0.0002	0.97	4.90	300	69.58	74.51	0.0004	0.99	3.42
400	142.20	150.99	0.0001	0.98	5.68	400	78.75	82.85	0.0004	0.99	1.88

Table 4
Langmuir and Freundlich model parameters and determination correlation coefficients for methylene blue and acid blue 29 adsorption on CS40CC60 at 30, 40 and 50 °C.

Dyes	Adsorption temperature (°C)	Langmuir isotherm				Freundlich isotherm			
		q_{max} (mg/g)	K_L (L/mg)	R^2	RMSE	K_F (mg/g).(L/mg)$^{1/n}$	n	R^2	RMSE
AB 29	30	132.04	0.27	0.78	23.71	59.58	5.71	0.96	10.68
	40	169.30	0.31	0.87	22.20	67.71	4.62	0.98	9.78
	50	167.35	7.06	0.95	15.32	105.06	6.10	0.94	16.65
MB	30	86.08	0.02	0.97	4.81	8.16	2.41	0.99	2.08
	40	88.27	0.03	0.91	8.88	9.24	2.45	0.98	4.64
	50	95.31	0.03	0.84	13.00	10.10	2.47	0.95	7.29

Plots of the experimental adsorption equilibrium data of MB and AB 29 on CS40CC60 together with the Langmuir and Freundlich models' fit at 30, 40 and 50 °C are illustrated in Fig. 5(c) and (d). The q_e increased gradually with increasing C_e thereby indicating an affinity for adsorption. Favorable adsorption and positive affinity in binding MB and AB 29 with the CS40CC60 surface at all the studied temperatures are also shown from the exponent n values in the Freundlich model (Table 4).

The significance of n is as follows: $n < 1$ (chemical process); $n = 1$ (linear); $n > 1$ (a physical process) [36]. As temperature increased from 30 °C to 50 °C, the n values varied from 5.71 to 6.10 for AB 29 and from 2.41 to 2.47 for MB indicating the favorable and physical adsorption of the dyes on the CS40CC60. Furthermore, for AB 29, the q_{max}, K_L, and K_F were 132.04 mg/g, 0.27 L/mg, and 59.58 (mg/g).(L/mg)$^{1/n}$, respectively, at 30 °C. However, they increased to 167.35 mg/g, 7.06 L/

Table 5
Comparison of the maximum monolayer adsorption capacities (mg/g) of different adsorbents for the removal of methylene blue and acid blue 29 adsorption.

| Adsorbents	Dye	Monolayer adsorption capacity q_{max} (mg/g)	References
Epichlorohydrin crosslinked chitosan/carbon–clay (CS40CC60)	Methylene blue	86.08	This work
	Acid blue 29	132.04	
Active MgO-SiO$_2$ hybrid material	Acid blue 29	44.90	[40]
	Methylene blue	126.10	
Activated olive pomace boiler ash	Methylene blue	149.11	[34]
	Acid blue 29	38.48	
Activated carbon-clay composite	Methylene blue	178.64	[15]
	Acid blue 29	104.83	
Cross-linked chitosan/activated oil palm ash zeolite	Methylene blue	151.51	[10]
	Acid blue 29	212.76	
Chitosan flakes activated carbon	Methylene blue	121.45	[42]
Magnetic chitosan/clay beads	Methylene blue	82.00	[39]
Chitin/clay microspheres	Methylene blue	152.20	[43]
Magnetic nanocomposite of chitosan/SiO$_2$/carbon nanotubes	Reactive blue 19	97.08	[38]
Chitosan/silica/zinc oxide nanocomposite	Methylene blue	293.30	[41]

AB 29 **MB**
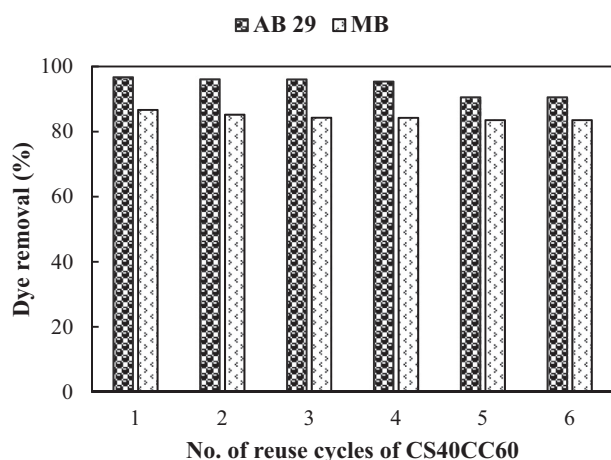
Fig. 6. Reuse cycles of CS40CC60 for dyes adsorption.

mg, and 105.06 $(mg/g).(L/mg)^{1/n}$ at 50 °C. These observations were consistent with the results obtained for MB. Thus, adsorbate molecules diffusion rate is promoted by increasing the temperature through the external boundary layer and within the pores. Based on the R^2 and RMSE in Table 4, the Freundlich isotherm model fit the results well compared to Langmuir isotherm. Also, the observed endothermic adsorption was attributed to a heterogeneous surface structure [37].

3.6. Performance and reusability of CS40CC60

The equilibrium adsorption capacities of CS40CC60 for MB and AB 29 were compared to other adsorbents reported in the literature and listed in Table 5. It is clear that CS40CC60 has reasonably good adsorption performance for both dyes compared to the reported [10,15,34,38–43]. Furthermore, the reusability of the CS40CC60 was explored by using ethanol solution as shown in Fig. 6. After CS40CC60 being used for six times, a slight decrease in MB removal (from 96.70% to 90.53%) and AB 29 removal (86.67% to 83.53%) were observed. These results prove that CS40CC60 has excellent reusability. Thus, CS40CC60 can be considered an economical and efficient adsorbent for dye-containing wastewater.

4. Conclusion

Epichlorohydrin crosslinked chitosan/carbon–clay (CS40CC60) biohybrid adsorbent was successfully prepared from chitosan (CS) and carbon–clay (CC) derived from the carbonization of spent bleaching sorbent for the removal of MB and AB 29 from aqueous solution. The CS40CC60 adsorption capacity was 86.08 mg/g for MB and 132.04 mg/g for AB 29 at 30 °C. The kinetic and isotherm data for the adsorption of both dyes onto CS40CC60 fit well to the pseudo-second-order model and the Freundlich isotherm. The CS40CC60 was successfully reused for six cycles with slight decrease for both dyes removals. The adsorption results revealed that the prepared CS40CC60 is an effective biohybrid adsorbent for MB and AB 29.

CRediT author statement

F. Marrakchi: Methodology, Formal analysis, Data curation, Writing - original draft. **B.H. Hameed:** Supervision, Conceptualization, Methodology, Validation, Writing - review & editing. **E.H. Hummadi:** Validation, Writing - review & editing.

Acknowledgements

References

[1] P.J. Landrigan, R. Fuller, N.J.R. Acosta, O. Adeyi, R. Arnold, N. (Nil) Basu, A.B. Baldé, R. Bertollini, S. Bose-O'Reilly, J.I. Boufford, P.N. Breysse, T. Chiles, C. Mahidol, A.M. Coll-Seck, M.L. Cropper, J. Fobil, V. Fuster, M. Greenstone, A. Haines, D. Hanrahan, D. Hunter, M. Khare, A. Krupnick, B. Lanphear, B. Lohani, K. Martin, K.V. Mathiasen, M.A. McTeer, C.J.L. Murray, J.D. Ndahimananjara, F. Perera, J. Potočnik, A.S. Preker, J. Ramesh, J. Rockström, C. Salinas, L.D. Samson, K. Sandilya, P.D. Sly, K.R. Smith, A. Steiner, R.B. Stewart, W.A. Suk, O.C.P. van Schayck, G.N. Yadama, K. Yumkella, M. Zhong, The Lancet Commission on pollution and health, Lancet 391 (2018) 462–512.
[2] Z. Yan, H. Yang, H. Dong, B. Ma, H. Sun, T. Pan, R. Jiang, R. Zhou, J. Shen, J. Liu, G. Lu, Occurrence and ecological risk assessment of organic micropollutants in the lower reaches of the Yangtze River, China: a case study of water diversion, Environ. Pollut. 239 (2018) 223–232.
[3] R. Sivashankar, A.B. Sathya, K. Vasantharaj, V. Sivasubramanian, Magnetic composite an environmental super adsorbent for dye sequestration – a review, Environ. Nanotechnol. Monit. Manag. 1 (2) (2014) 36–49.
[4] F. Piri, A. Mollahosseini, A. khadir, M. Milani Hosseini, Enhanced adsorption of dyes on microwave-assisted synthesized magnetic zeolite-hydroxyapatite nanocomposite, J. Environ. Chem. Eng. 7 (2019), 103338. .
[5] I. Ali, Water treatment by adsorption columns: evaluation at ground level, Sep. Purif. Rev. 43 (2014) 175–205.
[6] N.A. Rashidi, S. Yusup, A review on recent technological advancement in the activated carbon production from oil palm wastes, Chem. Eng. J. 314 (2017) 277–290.
[7] R. and Markets, Activated Carbon Market 2016–2022 - A Global Market Overview of thr $5.2 Billion Industry, GlobeNewswire News Room, 2016.
[8] L. Zhang, Y. Zeng, Z. Cheng, Removal of heavy metal ions using chitosan and modified chitosan: a review, J. Mol. Liq. 214 (2016) 175–191.
[9] Z.M. Şenol, N. Gürsoy, S. Şimşek, A. Özer, N. Karakuş, Removal of food dyes from aqueous solution by chitosan-vermiculite beads, Int. J. Biol. Macromol. 148 (2020) 635–646.
[10] W.A. Khanday, M. Asif, B.H. Hameed, Cross-linked beads of activated oil palm ash zeolite/chitosan composite as a bio-adsorbent for the removal of methylene blue and acid blue 29 dyes, Int. J. Biol. Macromol. 95 (2017) 895–902.
[11] F. Marrakchi, W.A. Khanday, M. Asif, B.H. Hameed, Cross-linked chitosan/sepiolite composite for the adsorption of methylene blue and reactive orange 16, Int. J. Biol. Macromol. 93 (2016) 1231–1239.
[12] M. Vakili, M. Rafatullah, B. Salamatinia, A.Z. Abdullah, M.H. Ibrahim, K.B. Tan, Z. Gholami, P. Amouzgar, Application of chitosan and its derivatives as adsorbents for dye removal from water and wastewater: a review, Carbohydr. Polym. 113 (2014) 115–130.
[13] A. Jimtaisong, T. Sarakonsri, Chitosan intercalated bentonite as natural adsorbent matrix for water-soluble sappanwood dye, Int. J. Biol. Macromol. 129 (2019) 737–743.
[14] M. Mana, M.S. Ouali, L.C. Menorval, J.J. Zajac, C. Charnay, Regeneration of spent bleaching earth by treatment with cethyltrimethylammonium bromide for application in elimination of acid dye, Chem. Eng. J. 174 (2011) 275–280.
[15] F. Marrakchi, M. Bouaziz, B.H. Hameed, Activated carbon–clay composite as an effective adsorbent from the spent bleaching sorbent of olive pomace oil: process optimization and adsorption of acid blue 29 and methylene blue, Chem. Eng. Res. Des. 128 (2017) 221–230.
[16] A. Benhouria, Md.A. Islam, H. Zaghouane-Boudiaf, M. Boutahala, B.H. Hameed, Calcium alginate–bentonite–activated carbon composite beads as highly effective adsorbent for methylene blue, Chem. Eng. J. 270 (2015) 621–630.
[17] E.M.S. Azzam, Gh. Eshaq, A.M. Rabie, A.A. Bakr, A.A. Abd-Elaal, A.E. El Metwally, S.M. Tawfik, Preparation and characterization of chitosan-clay nanocomposites for the removal of Cu(II) from aqueous solution, Int. J. Biol. Macromol. 89 (2016) 507–517.
[18] Y. Vijaya, S.R. Popuri, V.M. Boddu, A. Krishnaiah, Modified chitosan and calcium alginate biopolymer sorbents for removal of nickel (II) through adsorption, Carbohydr. Polym. 72 (2008) 261–271.
[19] M. Arora, N.K. Eddy, K.A. Mumford, Y. Baba, J.M. Perera, G.W. Stevens, Surface modification of natural zeolite by chitosan and its use for nitrate removal in cold regions, Cold Reg. Sci. Technol. 62 (2010) 92–97.
[20] Y. Peng, D. Chen, J. Ji, Y. Kong, H. Wan, C. Yao, Chitosan-modified palygorskite: preparation, characterization and reactive dye removal, Appl. Clay Sci. 74 (2013) 81–86.
[21] T. Ma, Y. Wu, N. Liu, Y. Wu, Hydrolyzed polyacrylamide modified diatomite waste as a novel adsorbent for organic dye removal: adsorption performance and mechanism studies, Polyhedron 175 (2020), 114227. .
[22] E. Altıntıg, H. Altundag, M. Tuzen, A. Sarı, Effective removal of methylene blue from aqueous solutions using magnetic loaded activated carbon as novel adsorbent, Chem. Eng. Res. Des. 122 (2017) 151–163.
[23] E.N. Seyahmazegi, R. Mohammad-Rezaei, H. Razmi, Multiwall carbon nanotubes decorated on calcined eggshell waste as a novel nano-sorbent: application for anionic dye Congo red removal, Chem. Eng. Res. Des. 109 (2016) 824–834.
[24] C. de G. Sampaio, L.S. Frota, H.S. Magalhães, L.M.U. Dutra, D.C. Queiroz, R.S. Araújo, H. Becker, J.R.R. de Souza, N.M.P.S. Ricardo, M.T.S. Trevisan, Chitosan/mangiferin particles for Cr(VI) reduction and removal, Int. J. Biol. Macromol. 78 (2015) 273–279.

[25] H. Gecol, P. Miakatsindila, E. Ergican, S.R. Hiibel, Biopolymer coated clay particles for the adsorption of tungsten from water, Desalination 197 (2006) 165–178.

[26] E.I. Unuabonah, A. Adewuyi, M.O. Kolawole, M.O. Omorogie, O.C. Olatunde, S.O. Fayemi, C. Günter, C.P. Okoli, F.O. Agunbiade, A. Taubert, Disinfection of water with new chitosan-modified hybrid clay composite adsorbent, Heliyon 3 (2017), e00379. .

[27] T.-Y. Kim, S.-S. Park, S.-Y. Cho, Adsorption characteristics of Reactive Black 5 onto chitosan beads cross-linked with epichlorohydrin, J. Ind. Eng. Chem. 18 (2012) 1458–1464.

[28] M. Auta, B.H. Hameed, Acid modified local clay beads as effective low-cost adsorbent for dynamic adsorption of methylene blue, J. Ind. Eng. Chem. 19 (2013) 1153–1161.

[29] S. Lagergren, About the Theory of So-called Adsorption of Soluble Substances, Kungliga Svenska Vetenskapsakademies Handlingar, 1898 1–39.

[30] Y.S. Ho, G. McKay, Pseudo-second order model for sorption processes, Process Biochem. 34 (1999) 451–465.

[31] I. Langmuir, The constitution and fundamental properties of solids and liquids. Part I. Solids, J. Am. Chem. Soc. 38 (1916) 2221–2295.

[32] H.M.F. Freundlich, Over the adsorption in solution, J. Phys. Chem. 57 (1906) 385–470.

[33] M. Auta, B.H. Hameed, Preparation of waste tea activated carbon using potassium acetate as an activating agent for adsorption of Acid Blue 25 dye, Chem. Eng. J. 171 (2011) 502–509.

[34] F. Marrakchi, M. Bouaziz, B.H. Hameed, Adsorption of acid blue 29 and methylene blue on mesoporous K_2CO_3-activated olive pomace boiler ash, Colloids Surf. A Physicochem. Eng. Asp. 535 (2017) 157–165.

[35] S. Noreen, H.N. Bhatti, M. Iqbal, F. Hussain, F.M. Sarim, Chitosan, starch, polyaniline and polypyrrole biocomposite with sugarcane bagasse for the efficient removal of Acid Black dye, Int. J. Biol. Macromol. 147 (2020) 439–452.

[36] X. Hu, H. Zhang, Z. Sun, Adsorption of low concentration ceftazidime from aqueous solutions using impregnated activated carbon promoted by Iron, Copper and Aluminum, Appl. Surf. Sci. 392 (2017) 332–341.

[37] Y. Xue, P. Xiang, H. Wang, Y. Jiang, Y. Long, H. Lian, W. Shi, Mechanistic insights into selective adsorption and separation of multi-component anionic dyes using magnetic zeolite imidazolate framework-67 composites, J. Mol. Liq. 296 (2019), 111990. .

[38] M. Abbasi, Synthesis and characterization of magnetic nanocomposite of chitosan/SiO_2/carbon nanotubes and its application for dyes removal, J. Clean. Prod. 145 (2017) 105–113.

[39] A. Bée, L. Obeid, R. Mbolantenaina, M. Welschbillig, D. Talbot, Magnetic chitosan/clay beads: a magsorbent for the removal of cationic dye from water, J. Magn. Magn. Mater. 421 (2017) 59–64.

[40] F. Ciesielczyk, P. Bartczak, J. Zdarta, T. Jesionowski, Active MgO-SiO_2 hybrid material for organic dye removal: a mechanism and interaction study of the adsorption of C.I. Acid Blue 29 and C.I. Basic Blue 9, J. Environ. Manag. 204 (2017) 123–135.

[41] H. Hassan, A. Salama, A.K. El-ziaty, M. El-Sakhawy, New chitosan/silica/zinc oxide nanocomposite as adsorbent for dye removal, Int. J. Biol. Macromol. 131 (2019) 520–526.

[42] F. Marrakchi, M.J. Ahmed, W.A. Khanday, M. Asif, B.H. Hameed, Mesoporous-activated carbon prepared from chitosan flakes via single-step sodium hydroxide activation for the adsorption of methylene blue, Int. J. Biol. Macromol. 98 (2017) 233–239.

[43] R. Xu, J. Mao, N. Peng, X. Luo, C. Chang, Chitin/clay microspheres with hierarchical architecture for highly efficient removal of organic dyes, Carbohydr. Polym. 188 (2018) 143–150.